MDPI

Multi-Extremum Adaptive Fuzzy Network Method for Dynamic Reliability Estimation Method of Vectoring Exhaust Nozzle

Chunyi Zhang [1], **Zheshan Yuan** [2,*], **Huan Li** [3], **Jiongran Wen** [3], **Shengkai Zheng** [1] **and Chengwei Fei** [3,*]

1   College of Mechanical and Electrical Engineering, Guangdong University of Science and Technology, Dongguan 523668, China; zhangchunyi@hrbust.edu.cn (C.Z.); 15627275559@163.com (S.Z.)
2   Weihai Guangtai Airport Equipment Co., Ltd., Weihai 264203, China
3   Department of Aeronautics and Astronautics, Fudan University, Shanghai 200433, China; 22110290013@m.fudan.edu.cn (H.L.); 20210290016@fudan.edu.cn (J.W.)
*   Correspondence: zheshan_yuan@163.com (Z.Y.); cwfei@fudan.edu.cn (C.F.)

Abstract: To enhance the accuracy and efficiency of reliability analysis for an aero-engine vectoring exhaust nozzle (VEN), a multi-extremum adaptive fuzzy network (MEAFN) method is developed by absorbing an adaptive neuro-fuzzy inference system (ANFIS) into the multi-extremum surrogate model (MESM) method. In the proposed method, the MERSM is used to establish the surrogate models of many output responses for the multi-objective integrated reliability analysis of the VEN. The ANFIS method is regarded as the basis function of the MESM method and adopted to improve the modeling precision of the MESM by introducing the membership degree into the input parameters and weights to improve the approximation capability of the neural network model to the high nonlinear reliability analysis of the VEN. The mathematical model of the MEAFN method and reliability analysis thoughts of the VEN is provided in this study. Then, the proposed MEAFN method is applied to conduct the dynamic reliability analysis of the expansion sheet and the triangular connecting rod in the VEN by considering the aerodynamic loads, operation temperature, and material parameters as the random input variables and the stresses and deformations as the output responses, compared with the Monte Carlo method and the extremum response surface method. From the comparison of the methods, it is indicated that the MEAFN method is promising to improve computational efficiency while maintaining accuracy. The efforts of this study provide guidance for the optimization design of the VEN and enrich the reliability theory of the flexible mechanism.

Keywords: vectoring exhaust nozzle; multi-extremum adaptive fuzzy network; reliability estimation; extremum response surface method

1. Introduction

To improve the accuracy and efficiency of reliability analysis for complex mechanical systems, researchers have proposed various methods based on the response surface method (RSM), such as the quadratic function response surface method [1], the support vector machine (SVM) response surface method [2,3], the Kriging-model-based response surface method [4], the artificial neural network-based response surface method [5], the stochastic response surface method [6], the extremum response surface method [7], and the fuzzy response surface method [8–10]. Later, some researchers combined other algorithms with the response surface method and developed various computational methods for reliability analysis. Zhang et al. [11] proposed a fuzzy and P-box hybrid variable turbine disk reliability estimation method based on equivalent entropy transformation and saddle point approximation, which reduced the required sample size and computational cost by using entropy invariance to transform fuzzy variables with a non-normal membership into normal random variables and applying SPA. Zhang et al. [12] integrated the AdaBoost algorithm with the BP neural network model and proposed an improved BP-AdaBoost algorithm model to conduct a diagnosis for the compound fault of gearboxes. Xu et al. [13]

considered the fuzziness of input random variables in mechanism reliability analysis and used the equivalent transformation principle to transform the input random variables with fuzzy distribution, and combined with the first-order second-moment (FOSM) method, they performed fatigue life reliability analysis for an aero-engine. Lopez et al. [14] found poor accuracy and convergence of the FOSM reliability method and proposed a class of fully probabilistic characteristics methods that could improve these defects. Eshghi et al. [15] proposed an adaptive improved surrogate model based on the response surface method, which combined the least-squares method with a new weight function to achieve adaptability, and applied it to saturated design and central composite design. Zhu et al. [16] combined the Gaussian regression function and response surface theory and proposed a Gaussian regression response surface, which was applied to civil engineering slope reliability analysis. Fei et al. [17] proposed a distributed collaborative extremum method based on the quadratic polynomial response surface model for complex turbine mechanical probabilistic analysis with high-performance and high-reliability high-pressure turbine blade-tip radial clearance probability analysis as the background. Zhai et al. [18] combined the improved response surface model with the static test and the Monte Carlo method to propose a stochastic model updating strategy for improving the accuracy and efficiency of the complex structure calculation model, and studied the reliability of a simply supported beam and aero-engine stator system. Du et al. [19] established a mathematical model of structural fuzzy reliability using the fuzzy random probability method, selected the optimal membership function, and proposed a direct integration method based on a dual neural network for the problem of the difficult multiple integration calculation in the fuzzy reliability mathematical model, which solved the structural fuzzy reliability problem with multidimensional random variables well and had high computational efficiency and accuracy. Xiao et al. [20] used existing relevant reliability data to perform error comparison analysis on test set data, conducted simulation training, and established a three-layer continuous optimization feedforward neural network model for the reliability prediction of a CNC machine tool spindle. Compared with the BP neural network, it has a faster learning speed and better nonlinear fitting ability. Abbasi et al. [21] extended the idea of rational linear patchy fuzzy numbers and introduced fuzzy arithmetic operations between two rational linear patchy fuzzy numbers, in which the reliability of each component is represented by a rational linear patchy fuzzy number. This method is more flexible and intelligent for modeling and analyzing the reliability of fuzzy systems. Nie et al. [22] represented the fuzzy characteristic parameters of structural fuzzy random variables as the sum of their true values and fuzzy perturbations, selected equivalent perturbations, and decomposed the probability density function and performance function into a series of intervals under different level cut sets. Then, based on the direct integration method, a sigmoid function was introduced to approximate the step function in the reliability function, and fuzzy reliability was obtained. The effectiveness and accuracy of this method were verified by simulation. Zhang et al. [23–25] successively proposed various improved the intelligent response surface method, the intelligent extremum response surface method, the distributed collaborative generalized regression extremum neural network method, the generalized regression extremum neural network method, and the particle swarm optimization–advanced extremum response surface method (PSO-AERSM). Keshtegar et al. [26] proposed a multi-extremum modified response basis model for the nonlinear response prediction of a dynamic turbine blisk. These methods were applied to turbine tip clearance reliability evaluation, blade LCF life reliability and sensitivity analysis under thermal–structural interaction, and flexible mechanism reliability analysis and optimization, improving the calculation accuracy and efficiency. Li et al. [27] integrated the advantages of the improved differential evolution (IDE) algorithm and neural network model into the decomposition coordination strategy, and proposed a multi-agent collaborative modeling (MACM) method. They took a typical turbine rotor as an engineering example for fatigue reliability estimation. This method improved the calculation accuracy and simulation efficiency of turbine rotor fatigue reliability estimation. Song et al. [28,29] combined fuzzy reliability theory, a neural network

metamodel, and distributed coordination strategy, and proposed a distributed coordination neural network metamodel and advanced multiple response surface method. They performed probabilistic low-cycle fatigue estimation and sensitivity analysis on turbine disks, improving the calculation efficiency and accuracy of the probabilistic low-cycle fatigue estimation of turbine disks. The extensive research on response surface method theory by these scholars improved the calculation accuracy and efficiency of reliability analysis, and promoted the development of mechanical system reliability analysis theory.

Due to the great uncertainty of the parameters of the flexible mechanism (e.g., vectoring exhaust nozzle) in the process of motion, the fuzziness of the system increases sharply. After investigation, there are few studies on the reliability analysis of flexible mechanisms, and no accurate and effective reliability analysis method has been formed to solve the problems of fuzziness and dynamics.

In this paper, the multi-extremum adaptive fuzzy network (MEAFN) method is proposed by absorbing the adaptive neuro-fuzzy inference system (ANFIS) into the multi-extremum surrogate model (MESM). In the proposed method, the MERSM is used to establish the surrogate models of many output responses for the multi-objective integrated reliability analysis of a vectoring exhaust nozzle (VEN). The ANFIS method is regarded as the basis function of the MESM method and adopted to improve the modeling precision of the MESM by introducing the membership degree into the input parameters and weights to improve the approximation capability of the neural network model to the high nonlinear reliability analysis of the VEN. The aerodynamic loads, operation temperature, and material parameters of the expansion sheet and the triangular connecting rod in the VEN are used as the random input variables and the stresses and deformations as the output responses. Compared with the Monte Carlo method (MCM) and the extremum response surface method (ERSM), the results indicated that the MEAFN method greatly improves the calculation efficiency under the premise of accuracy.

In what follows, Section 2 proposes the main theory and methods, including the MEAFN mathematical model, the reliability analysis thought with the MEAFN method, and the thermal–structural coupling analysis theory. Section 3 conducts the dynamic reliability analysis of the expansion sheet and the triangular connecting rod in the VEN to discuss the performance of the MEAFN method compared with the other methods. Section 4 gives a summary of the whole paper.

2. Theory and Methods

2.1. MEAFN Method

The proposed MEAFN method engages the strengths of the ANFIS and the MESM to conduct a dynamic reliability analysis of the flexible mechanism. The relevant basic methods will be introduced in this section.

2.1.1. Fuzzy Neural Network

The fuzzy neural network (FNN) is a theoretical method that integrates the structural knowledge representation ability of fuzzy logic reasoning and the self-learning ability of the neural network [30]. Essentially, the FNN introduces fuzzy input signals and fuzzy weights into conventional neural network models, such as the feedforward neural network [31] and the Hopfield neural network [32], to handle imprecise data and uncertainty.

The basic idea of a fuzzy neural network is to find the parameters of a fuzzy system (i.e., fuzzy sets and fuzzy rules) by the approximation of neural networks. A fuzzy set is a class of objects with a continuum of grades of membership, and is characterized by a membership function that assigns to each object a grade of membership ranging between [0, 1] instead of limiting to 0 or 1. A grade of membership indicates the degree to which an element belongs to a fuzzy set and measures how well an element satisfies the conditions for membership in a fuzzy set. Fuzzy rules are used within fuzzy logic systems to infer an output based on input variables. The rule base of a fuzzy system can be interpreted

as a neural network, where fuzzy sets can be regarded as weights, whereas the input and output variables and the rules are modeled as neurons.

Let X be a domain. Mapping $A(x) : X \to [0,1]$ determines a fuzzy subset A on X. $A(x)$ is called the membership function of A, and X belongs to the membership degree of A, that is,

$$\forall x \in X, \; A(x) \in [0,1] \tag{1}$$

The membership relation expression is:

$$\begin{cases} A(x) = 1 & X \text{ completely belongs to } A \\ A(x) = 0 & X \text{ not belongs to } A \\ 0 < A(x) < 1 & X \text{ partly belongs to } A \end{cases} \tag{2}$$

This paper employs the triangular membership function to calculate as

$$\mu(x) = e^{-\frac{x - x_0}{2\sigma^2}} \tag{3}$$

where x_0 is the mean of random variable x, and σ is the standard deviation of random variable x.

The membership function is the basis for the application of fuzzy sets to practical problems. For specific fuzzy objects, only by determining the actual membership function can the fuzzy theory be used to perform a specific quantitative analysis. Generally, a fuzzy neural network mainly uses a neural network structure to realize fuzzy logic reasoning, thus endowing the weights without clear physical meaning in traditional neural networks with the physical meaning of reasoning parameters in fuzzy logic.

2.1.2. Adaptive Neuro-Fuzzy Inference System

The artificial neural network (ANN) [33] is a computational model that mimics the structure and function of biological neural networks and has strong self-learning and adaptive ability, but it is similar to a black box, lacks transparency, and cannot express the reasoning function of the human brain. The fuzzy inference system (FIS) [34] is a mathematical model that uses fuzzy sets to represent the input and output variables of a system, but has no adaptive ability, which limits its application. Jang Roger [35] proposed the adaptive neuro-fuzzy inference system (ANFIS), which engages the advantages of the FIS and the ANN into a uniform solution to solve science and engineering problems.

In order to realize the learning process of the T-S fuzzy model [36], it is generally transformed into an adaptive network. The structure of the adaptive fuzzy neural network system is shown in Figure 1.
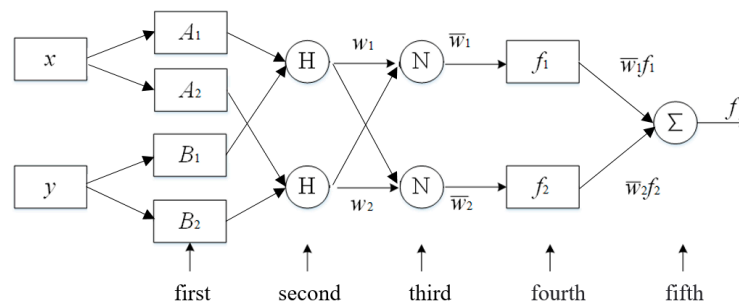

Figure 1. Structure of adaptive fuzzy neural network system.

The first layer (fuzzy layer) defines the fuzzy terms of input variables to fuzzifiers the random input variables. The output function of node i is

$$\begin{cases} O_i^1 = \mu A_i(x) & i = 1,2 \\ O_i^1 = \mu B_i(y) & i = 1,2 \end{cases} \tag{4}$$

where x and y are the input of node i; A_i and B_i are fuzzy sets; O_i^1 is the membership function value of A_i and B_i, representing the degree to which x and y belong to A_i and B_i; and the form of the membership function μA_i and μB_i is determined by the antecedent parameters.

$$O_i^2 = w_i = \mu A_i(x) \times \mu B_i(x) \quad i = 1, 2 \tag{5}$$

The third layer (normalized layer) normalizes the firing strengths of all rules.

$$O_i^3 = \overline{w} = \frac{w_i}{(w_1 + w_2)} \quad i = 1, 2 \tag{6}$$

The fourth layer (defuzzification layer) calculates the crisp output value from the normalized firing strengths of all rules.

$$O_i^4 = \overline{w}_i f_i = \overline{w}_i(p_i x + q_i x + r_i) \quad i = 1, 2 \tag{7}$$

where $\overline{w}_i$ is the output of the third layer, and $\{p_i, q_i, r_i\}$ is the consequent parameter set of the node.

The fifth layer (total output layer) sums up all crisp output values.

$$O_i^5 = \Sigma \overline{w}_i f_i = \frac{\Sigma w_i f_i}{\Sigma w_i} \quad i = 1, 2 \tag{8}$$

Given the antecedent parameters, the output of the ANFIS can be expressed as a linear combination of consequent parameters:

$$O_i^5 = \overline{w}_1 f_1 + \overline{w}_2 f_2 = (\overline{w}_1 x)p_1 + (\overline{w}_1 y)q_1 + \overline{w}_1 r_1 + (\overline{w}_2 x)p_2 + (\overline{w}_2 y)q_2 + \overline{w}_2 r_2 \tag{9}$$

The ANFIS combines fuzzy theory, which is easy to express human knowledge, with the ANN, which has distributed message storage and efficient adaptive learning ability. It provides a new method for fuzzy information processing in engineering practice.

2.1.3. The Mathematical Model of MEAFN Method

The MESM is to establish several extremum response surface functions based on the single extremum response surface method. For each set of input random variables, the corresponding multiple extreme output responses can be calculated, namely

$$\mathbf{X} = [x_i] \xrightarrow{\text{Calculate multi-extremum outputs}} \mathbf{Y} = [y_1 \ y_2 \ y_3 \cdots y_n] \tag{10}$$

Herein, $\mathbf{X}$ is the input random variable vector, and subscript $i = 1, 2, \ldots$ is the number of inputs; $\mathbf{Y}$ is the output response vector, and subscript $n = 1, 2, \ldots$ is the output response number. The extremum of each output response y_{max}^i is substituted into the response surface function formula, and the quadratic polynomial coefficient is obtained by the least-squares method. Then, the mathematical model of the multi-extremum response surface is established as shown in Equation (11).

$$\begin{cases} y_{max}^1 = b_0^1 + \sum_{i=1}^n b_i x_i + \sum_{i=1}^n \sum_{j=1}^n b_{ij}^1 x_i x_j \\ \quad\quad\quad\quad \vdots \\ y_{max}^n = b_0^n + \sum_{i=1}^n b_i x_i + \sum_{i=1}^n \sum_{j=1}^n b_{ij}^n x_i x_j \end{cases} \tag{11}$$

Combined with the stochastic function, the input random variable x is transformed by the Hermite polynomial, and then the mathematical model of the stochastic multi-extremum response surface is constructed as Equation (12).

$$
\begin{cases}
y_{\max}^1(\xi) = b_0^1 + \sum_{i=1}^n b_i^1 H_1\left(\xi_{i_1}\right) + \cdots + \sum_{i_1=1}^n \sum_{i_2=1}^{i_1} \cdots \sum_{i_p=1}^{i_{p-1}} b_{i_1 i_2 - i_p}^1 H_p\left(\xi_{i_1} \xi_{i_2} \cdots \xi_{i_p}\right) \\
\qquad\qquad\qquad\qquad\qquad \vdots \\
y_{\max}^n(\xi) = b_0^n + \sum_{i=1}^n b_i^n H_1\left(\xi_{i_1}\right) + \cdots + \sum_{i_1=1}^n \sum_{i_2=1}^{i_1} \cdots \sum_{i_p=1}^{i_{p-1}} b_{i_1 i_2 - i_p}^n H_p\left(\xi_{i_1} \xi_{i_2} \cdots \xi_{i_p}\right)
\end{cases}
\tag{12}
$$

where the value of $i_1, i_2, \ldots, i_p$ is $1, 2, \ldots, n$, b_0^n is the constant term, $b_i^n, b_{i_1}^n, b_{i_1 i_2}^n, b_{i_1 i_2 \cdots i_p}^n$ denote the polynomial coefficient, and $H_p(\xi_{i_1}, \xi_{i_2} \cdots \xi_{i_p})$ is a p-order Hermite polynomial, and its expression is

$$
H_p\left(\xi_{i_1}, \xi_{i_2} \cdots \xi_{i_p}\right) = (-1)^p e^{\frac{\xi^T \xi}{2}} \frac{\partial^p}{\partial \xi_{i_1} \partial \xi_{i_2} \cdots \partial \xi_{i_p}} \left(e^{-\frac{\xi^T \xi}{2}}\right)
\tag{13}
$$

where $\xi = \left(\xi_{i_1}, \xi_{i_2} \cdots \xi_{i_p}\right)$ indicate the vector formed by the i_p independent standard normal random variables.

2.2. Reliability Analysis with MEAFN Method

To enhance the efficiency and accuracy of structural dynamic reliability estimation, the MEAFN method is developed by absorbing the superiorities of both the AFNIS and the MESM into a surrogate model. The MESM is the basis input–output surrogate model of the multi-object system, which can handle the transient analysis process. The AFNIS method is the basis function of the MESM to structure a precise surrogate model for the structural dynamic reliability evaluation. In respect of the proposed MEAFN, the procedure of structural dynamic reliability estimation is shown in Figure 2.

As shown in Figure 2, the procedure of reliability analysis with the MEAFN method is summarized as follows:

***Step* 1:** Create a finite-element (FE) model of the objective structure and divide its mesh, and assign the boundary conditions, material properties, and loads within a time domain.

***Step* 2:** Extract the small batch random input variables by the MCM based on variable numerical characteristics, and perform the dynamic deterministic analysis of the objective structure based on the established FE model to compute the corresponding extreme outputs.

***Step* 3:** Take the random input variable x and the extreme output response y_{max}^i of the flexible system as the input and the output of the ANFIS, respectively. Then, establish the multi-failure output response Y:

$$
Y = [y_{max}^1, y_{max}^2, \cdots y_{max}^n]
\tag{14}
$$

***Step* 4:** Divide the input and output samples from the FE analysis into two sets: training set and testing set, which are loaded in the ANFIS editor.

***Step* 5:** Initialize the parameters of the fuzzy inference system (FIS), including membership functions and generating rules.

***Step* 6:** Train the initialized FIS structure by the ANFIS function with the training samples, validate the derived model by the evalfis and plot function with testing samples, and optimize the membership function. Then, establish the MEAFN model.

***Step* 7:** Use the MEAFN model instead of the limit state function for reliability analysis. Extract a large number of random input variable samples and substitute them into the MEAFN model to compute the corresponding output responses, and then compare the output responses with the corresponding allowable values to calculate the reliability of the objective structure.
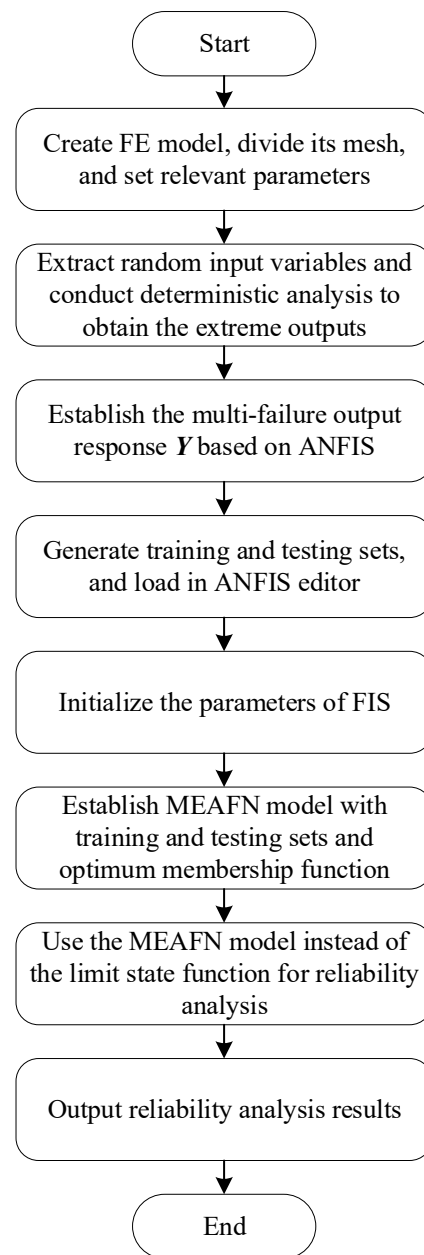
```
                          ┌──────────┐
                          │  Start   │
                          └──────────┘
                               │
                               ▼
              ┌─────────────────────────────────┐
              │ Create FE model, divide its mesh,│
              │    and set relevant parameters   │
              └─────────────────────────────────┘
                               │
                               ▼
              ┌─────────────────────────────────┐
              │  Extract random input variables and│
              │  conduct deterministic analysis to │
              │     obtain the extreme outputs     │
              └─────────────────────────────────┘
                               │
                               ▼
              ┌─────────────────────────────────┐
              │  Establish the multi-failure output│
              │     response Y based on ANFIS      │
              └─────────────────────────────────┘
                               │
                               ▼
              ┌─────────────────────────────────┐
              │  Generate training and testing sets,│
              │      and load in ANFIS editor      │
              └─────────────────────────────────┘
                               │
                               ▼
              ┌─────────────────────────────────┐
              │     Initialize the parameters of FIS│
              └─────────────────────────────────┘
                               │
                               ▼
              ┌─────────────────────────────────┐
              │   Establish MEAFN model with       │
              │   training and testing sets and    │
              │   optimum membership function      │
              └─────────────────────────────────┘
                               │
                               ▼
              ┌─────────────────────────────────┐
              │   Use the MEAFN model instead of   │
              │  the limit state function for reliability│
              │             analysis               │
              └─────────────────────────────────┘
                               │
                               ▼
              ┌─────────────────────────────────┐
              │   Output reliability analysis results│
              └─────────────────────────────────┘
                               │
                               ▼
                          ┌──────────┐
                          │   End    │
                          └──────────┘
```

Figure 2. Procedure of structural dynamic reliability estimation with MEAFN.

2.3. Thermal–Structural Coupling Analysis Theory

Thermal–structural coupling analysis is performed based on the realistic operating conditions of the VEN [37]. Thermal analysis studies how thermal loads affect structures, causing thermal stress and deformation. Structural analysis focuses on the stress and deformation of components under external loads. From take-off to landing, the VEN experiences high temperature, aerodynamic pressure, and other loads that affect its structural reliability. In the thermal–structural coupling analysis of the VEN, we first perform thermal analysis to obtain the temperature distribution, thermal deformation, and temperature field of the VEN structure under the thermal field. Then, we use the temperature field as an input load for the structural analysis of the VEN. In the structural analysis, we obtain the stress and deformation of the expansion sheet and the triangular connecting rod under thermal–structural coupling.

Based on the Fourier law of heat conduction and the law of the conservation of energy, the three-dimensional heat conduction equation (Equation (15)) is established.

$$c\rho \frac{\partial T}{\partial t} = \frac{\partial}{\partial x}(k\frac{\partial T}{\partial x}) + \frac{\partial}{\partial y}(k\frac{\partial T}{\partial y}) + \frac{\partial}{\partial z}(k\frac{\partial T}{\partial z}) \tag{15}$$

where $k = k(x, y, z)$ is the thermal conductivity of the component material at (x, y, z), c is the specific heat capacity of the component material, and ρ is the density of the component material.

The thermal analysis of the VEN is carried out by combining the thermal convection Newton cooling equation (Equation (16)) and the initial condition equation (Equation (17)). Then transferring the data of the thermal analysis are transferred to the surface of the structure with the FE method.

$$q^* = h_f(T_S - T_B) \tag{16}$$

in which h_f is the convective heat transfer coefficient, T_S is the surface temperature of the structure, and T_B is the temperature of the surrounding environment of the structure.

$$T_{t=0}(x, y, z) = T_0(x, y, z) \tag{17}$$

Herein, T_0 is the initial temperature of the structure when $t = 0$.

3. Dynamic Reliability Estimation of VEN

In this section, the dynamic reliability estimation of the VEN is completed by the proposed MEAFN, involving FE modeling, the determination of random variables, dynamic deterministic analysis, the validation of the MEAFN, and the comparison of methods.

3.1. FE Modeling

In the VEN, the force condition of the expansion sheet and the triangular connecting rod is the most complex. Therefore, the expansion sheet and the triangular connecting rod are the key research objects in the strength reliability analysis of the VEN. The FE models of the expansion sheet and the triangular connecting rod are shown in Figures 3 and 4.
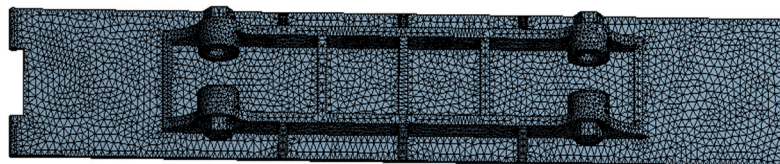
Figure 3. FE model of expansion sheet.
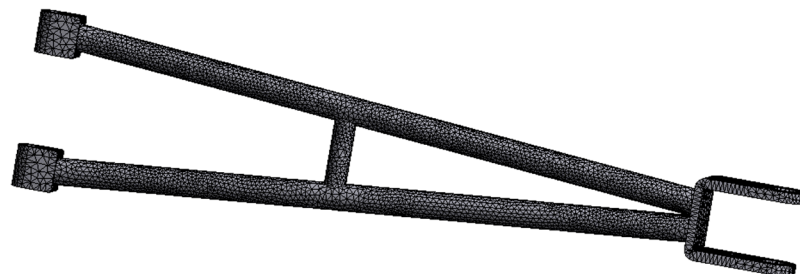
Figure 4. FE model of triangular connecting rod.

The FE models of the expansion sheet and the triangular connecting rod involve 75,826 tetrahedron elements and 286,514 vertices, as well as 28,997 elements and 108,904 nodes, respectively. These models will be employed for thermal–structural coupling analysis and reliability estimation.

3.2. Determination of Random Variables

In the analysis time domain [0 s, 0.3 s], the aerodynamic force of the VEN P, the material density of the expansion sheet ρ_1, the material density of the triangular connecting rod ρ_2, the elastic modulus of the expansion sheet E_1, and the elastic modulus of the triangular connecting rod E_2 are taken as the input random variables. Assuming that each random variable is independent of each other and obeys the normal distribution as shown in Table 1.

Table 1. Random variables in static reliability analysis of VEN.

Random Variables	Mean	Standard Deviation	Distribution
$P/(\text{Mpa})$	0.5	0.01	Normal
$T/(\text{K})$	873	26.29	Normal
$\rho_1/(\text{kg} \cdot \text{m}^{-3})$	8570	292.7	Normal
$\rho_2/(\text{kg} \cdot \text{m}^{-3})$	8240	287.1	Normal
$E_1/(\text{Gpa})$	202	6.06	Normal
$E_2/(\text{Gpa})$	205	6.15	Normal

3.3. Dynamic Deterministic Analysis

In the VEN, the operation environment of the expansion sheet is the worst, which bears huge gas pressure at high temperatures. In the process of nozzle folding, the stress level of some parts of the expansion sheet may even reach the yield limit of the material. The loads of the expansion sheet are mainly the aerodynamic pressure on the vertical bottom surface and concentrated load at the connection with the triangular connecting rod. The temperature distribution, stress, and deformation of the expansion sheet and the triangular connecting rod in the analysis time domain are obtained by thermal–structural coupling analysis, as shown in Figures 5–9.
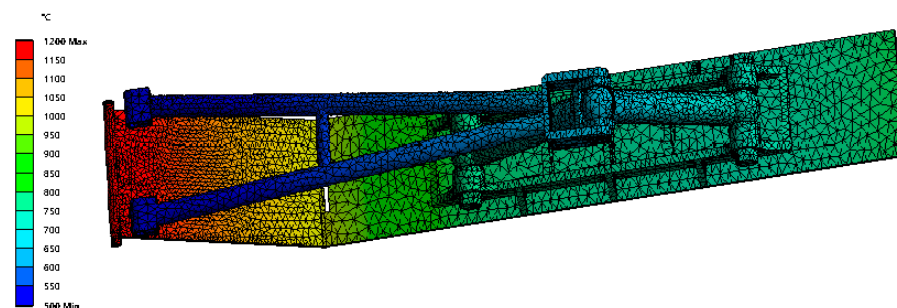
Figure 5. Temperature distribution of expansion sheet and triangular connecting rod.
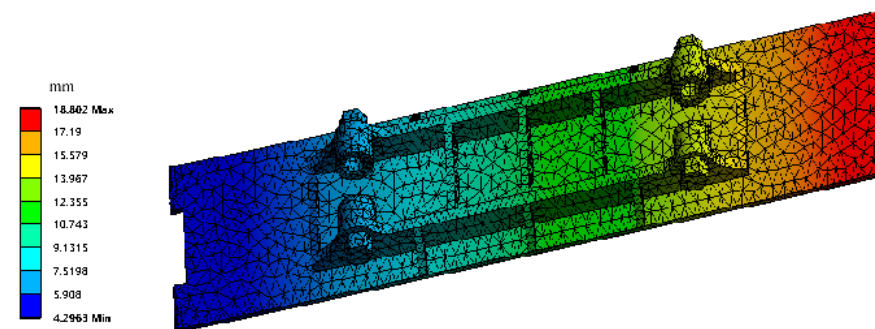
Figure 6. Deformation distribution of expansion sheet.

As seen from the results of the dynamic deterministic analysis, the maximum deformation of the expansion sheet reaches 18.8 mm, locating the end of the expansion plate; the maximum deformation of the triangular connecting rod is in the end of the drag link with

10.5 mm; the outer circle of the expansion plate and the drag link in the expansion sheet holds a maximum stress of 413.9 Mpa; and the stress in the hinge hole area at the top of the tie rod is the greatest with 2788.6 Mpa. These dangerous areas are focused on reliability estimation.
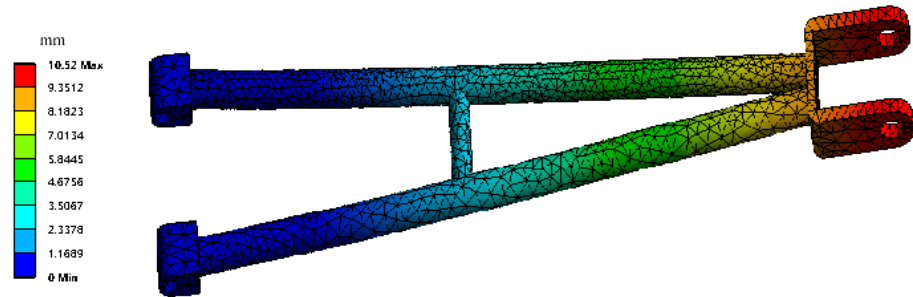

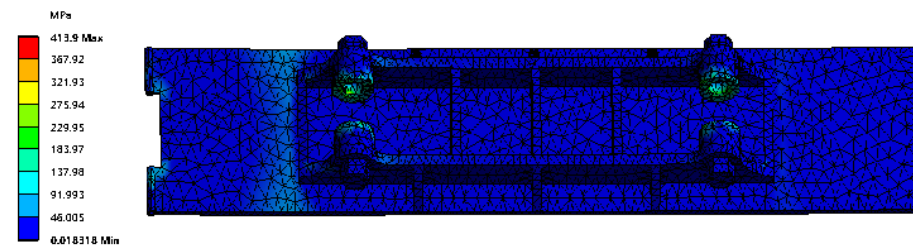**Figure 7.** Deformation distribution of triangular connecting rod.

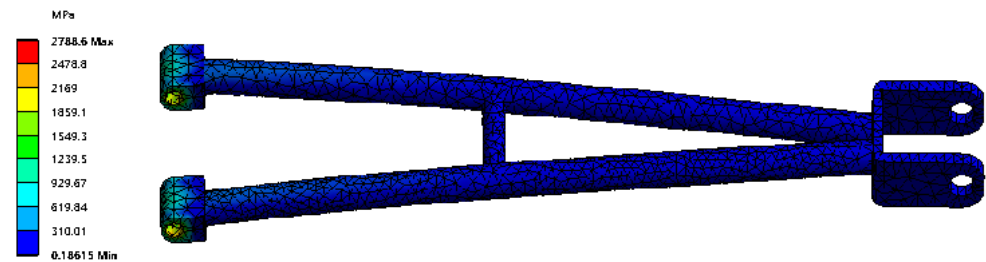**Figure 8.** Stress distribution of expansion sheet.

Figure 9. Stress distribution of triangular connecting rod.

3.4. Validation of MEAFN

We used the MCM to sample 100 groups of small batches of random input variables in Table 1, and obtained the output response by the CAE simulation calculation, that is, the maximum stress and maximum deformation value of the expansion blade and the triangular connecting rod in the analysis time domain. The input–output samples are substituted into Equation (12) to construct a mathematical model of the quadruple stochastic extremum response surface. We then used the MCM again to extract 80 groups from 100 groups of samples as training samples and the remaining 20 groups as testing samples. Substituting the training samples into the triangle membership function (Equation (3)), calculating the attribution area value of the sample points, and dividing the attribution area, the calculation results are as follows:

$$\mu A_1(x) = \begin{bmatrix} 0.7068 & 0.8245 & \cdots & 0.7534 \\ 0.9862 & 0.9025 & \cdots & 0.9352 \\ 0.7240 & 0.8026 & \cdots & 0.8762 \\ 0.6002 & 0.6584 & \cdots & 0.9925 \\ 0.8267 & 0.8362 & \cdots & 0.8260 \\ 0.9026 & 0.8635 & \cdots & 0.8950 \end{bmatrix}_{6 \times 40} \tag{18}$$

$$\mu A_2(x) = \begin{bmatrix} 0.6065 & 0.5298 & \cdots & 0.5983 \\ 0.7259 & 0.7907 & \cdots & 0.7752 \\ 0.6825 & 0.5867 & \cdots & 0.6530 \\ 0.5682 & 0.5902 & \cdots & 0.4996 \\ 0.7852 & 0.7216 & \cdots & 0.7018 \\ 0.8490 & 0.7925 & \cdots & 0.6894 \end{bmatrix}_{6 \times 40} \tag{19}$$

$$\mu B_1(y) = \begin{bmatrix} 0.9581 & 0.8659 & \cdots & 0.9327 \\ 0.8951 & 0.8526 & \cdots & 0.9247 \\ 0.9120 & 0.9024 & \cdots & 0.9571 \\ 0.9238 & 0.9859 & \cdots & 0.9005 \end{bmatrix}_{4 \times 40} \tag{20}$$

$$\mu B_2(y) = \begin{bmatrix} 0.8543 & 0.8267 & \cdots & 0.8109 \\ 0.8356 & 0.7583 & \cdots & 0.8206 \\ 0.8725 & 0.8700 & \cdots & 0.7999 \\ 0.7958 & 0.8254 & \cdots & 0.8367 \end{bmatrix}_{4 \times 40} \tag{21}$$

Substituting the results into Equations (4)–(9), the MEAFN method model is established. The testing samples are substituted into the MEAFN model to optimize the membership function. The optimization results are shown in Figure 10. The evaluation and prediction results are shown in Figures 11 and 12. It can be seen that the trained membership fuzzy set has been improved, and the prediction results of the MEAFN method are basically consistent with the original data.

(a)

(b)
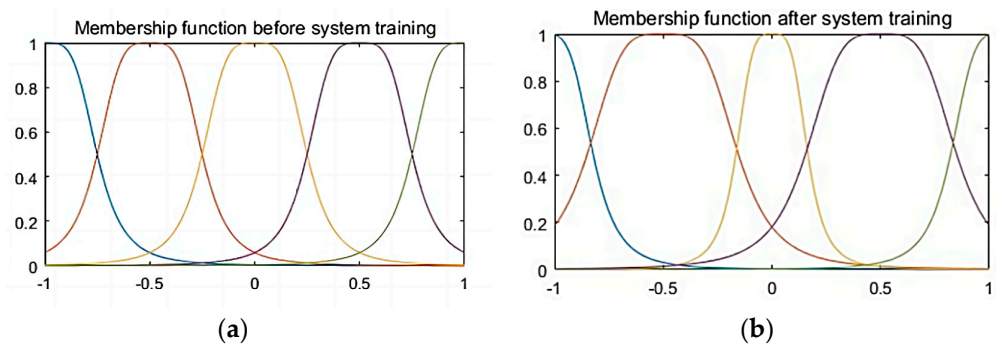
Figure 10. Membership function optimization diagram: (**a**) Before optimization; (**b**) After optimization.

(a)

(b)
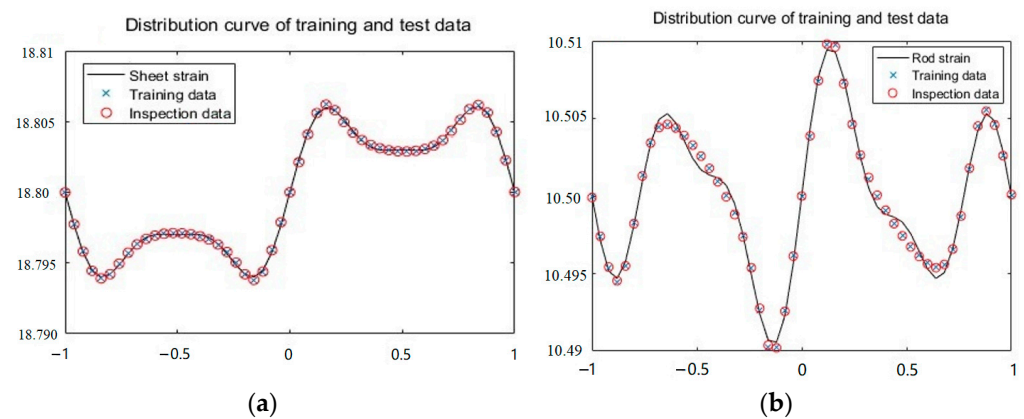
Figure 11. Deformation training and inspection curve: (**a**) Expansion sheet; (**b**) Triangular connecting rod.
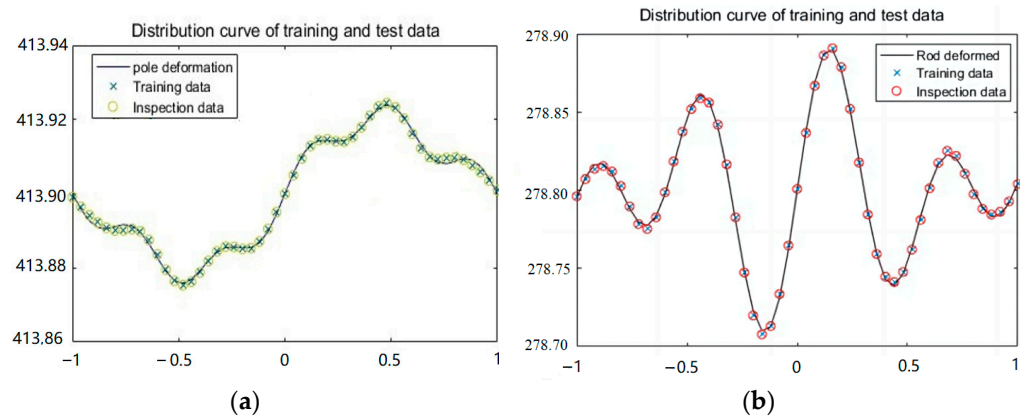
Figure 12. Stress training and inspection curve: (**a**) Expansion sheet; (**b**) Triangular connecting rod.

We performed 10,000 linkage sampling of the MEAFN mathematical model using the MCM to obtain the simulation sampling plots and frequency histograms of the maximum deformation and maximum stresses of the expansion sheet and the triangular connecting rod in the analysis time domain, as shown in Figures 13–16.
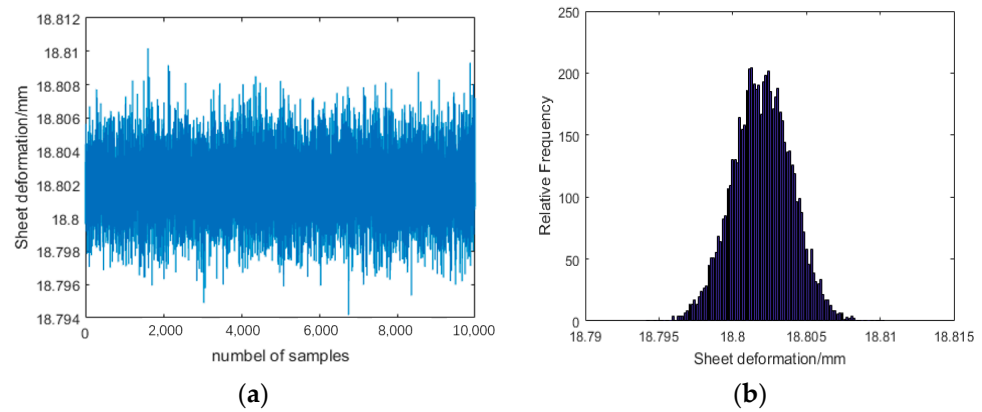

Figure 13. Expansion sheet deformation: (**a**) Simulation sampling diagram; (**b**) Frequency histogram.
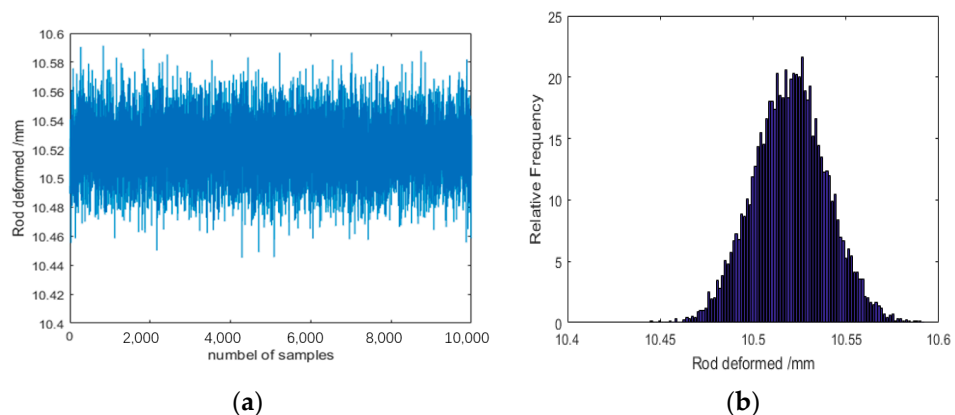
Figure 14. Triangular connecting rod deformation: (**a**) Simulation sampling diagram; (**b**) Frequency histogram.

From Figures 13–16, it can be seen that the output variables meet the normal distribution. The mean values of deformation and stress of the expansion sheet obtained by reliability analysis are 18.8037 and 413.9684, respectively, and the corresponding standard deviations are 4.5616×10^{-4} and 4.6831×10^{-4}, respectively. The mean values of defor-

mation and stress of the triangular connecting rod are 10.5197 and 278.8566, while the corresponding standard deviations are 3.9755×10^{-4} and 3.4467×10^{-4}. In the process of 10,000 simulations, the number of failures is 57, the reliability is 0.9943, and the calculation time is 2.300 s.
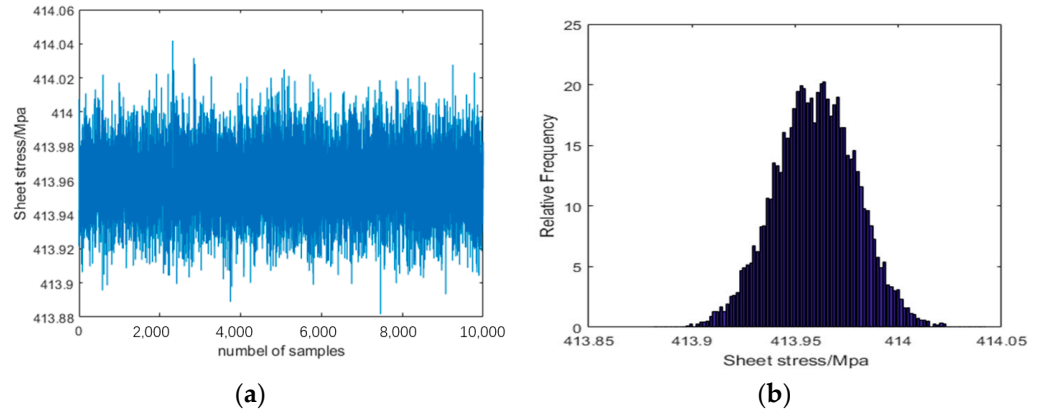

Figure 15. Expansion sheet stress: (**a**) Simulation sampling diagram; (**b**) Frequency histogram.
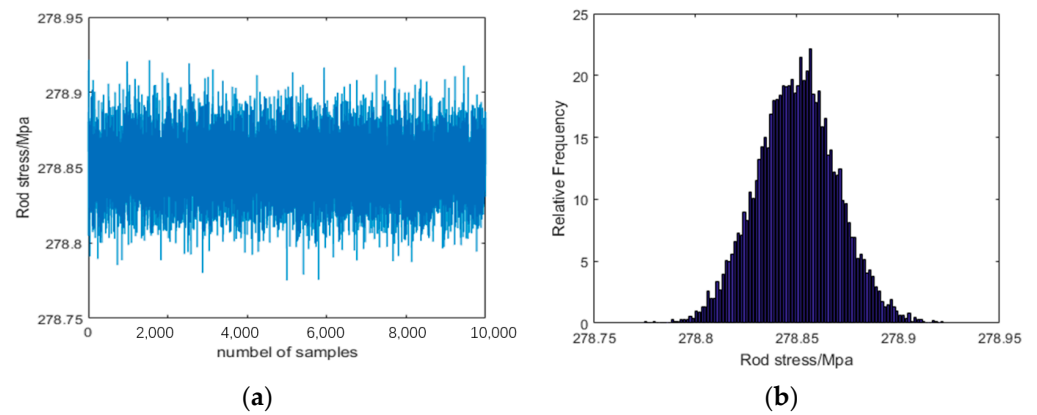

Figure 16. Triangular connecting rod stress: (**a**) Simulation sampling diagram; (**b**) Frequency histogram.

3.5. Comparison of Methods

The MCM, ERSM, and MEAFN methods are used to analyze the multi-objective coupling failure mode probability of the deformation and stress of the expansion sheet and the triangular connecting rod under the same simulation conditions. With the increase in simulation times, the computing accuracy and time of different methods are shown in Tables 2 and 3.

Table 2. The accuracy of calculating reliability by different methods.

Number of Samples	Reliability/%		
	MCM	**ERSM**	**MEAFN**
10^2	98	96	98
10^3	99.1	97.5	98.9
10^4	—	98.69	99.43
10^5	—	—	99.86

Table 3. The time of calculating reliability by different methods.

Number of Samples	Time/s		
	MCM	**ERSM**	**MEAFN**
10^2	8651	1.25	0.62
10^3	196,829	4.58	0.98
10^4	—	10.29	2.30
10^5	—	—	3.82

4. Discussion

Since the MCM is calculated by the full FE model simulation, its results are usually used as a standard for comparison with other methods. Compared with the other methods, the results of dynamic reliability estimation with the MEAFN are almost consistent with those of the MCM under the same simulations, and are superior to the other methods from Table 2. The computational advantages of the MEAFN method become increasingly apparent as the increase in simulation times. As shown in Table 3, the MCM cannot perform 10^4 simulations due to the huge computational cost, while the MEAFN keeps the fast computation speed and is faster than the other methods. So, it has a good prospect.

5. Conclusions

The aim of this study is to propose the multi-extremum adaptive fuzzy network (MEAFN) method by absorbing an adaptive neuro-fuzzy inference system (ANFIS) into a multi-extremum surrogate model (MESM) to enhance the accuracy and efficiency of the reliability analysis for an aero-engine vectoring exhaust nozzle (VEN). In the developed method, the MESM is applied to establish the surrogate models of many output responses for the multi-objective integrated reliability analysis of the VEN. The ANFIS is employed to improve the modeling precision of the MESM by introducing the membership degree into the input parameters and weights. Through the dynamic reliability analysis of the VEN, some main conclusions are summarized as follows:

(1) Through dynamic deterministic analysis of the VEN within the time domain based on thermal–structural coupling theory, the maximum deformation and maximum stress values of the expansion sheet and the triangular connecting rod were 18.802 mm, 413.9 Mpa, and 10.52 mm, 27.89 Mpa, respectively.

(2) The multi-objective coupling failure mode probability of the deformation and stress of the expansion sheet and the triangular connecting rod is about 98.9% with the MEAFN under 10^3 simulations, which offers a reference for the reliability design of the VEN in engineering.

(3) The MEAFN method is highly efficient and precise in the dynamic reliability analysis of the VEN. This is because the MEAFN combines the advantages of the MESM and the ANFIS. The extremum thought can handle the dynamic problem and reduce the workload of modeling, and the multi-surrogate model has strength in computing the reliability degree of the multi-failure modes in the MESM. As the basis function of the MESM model, the ANFIS is a combination of the adaptive neural network (ANN) and the fuzzy inference system (FIS), which inherits the interpretability of the FIS and the learning ability of the ANN to improve the efficiency and accuracy of the MEAFN.

(4) The performance of the MEAFN is validated in a case study of the VEN. Compared with the other three methods, the results of dynamic reliability estimation with the MEAFN are almost consistent with those of the Monte Carlo method (MCM) under the same simulations, and are superior to other methods. With the increase in simulation times, the advantage of simulation efficiency of the MEAFN becomes more prominent. In particular, the MCM cannot perform 10^4 simulations due to the huge computational cost, while the MEAFN keeps the fast computation speed and is faster than the other methods.

The efforts of this study provide a high-precision and high-efficient approach (MEAFN), which offers guidance for the optimization design of the VEN and enriches the reliability theory of the flexible mechanism.

Along with the reliability analysis method of the flexible mechanisms, some advanced methods will be developed based on more advanced algorithms (particle swarm optimization, Marine predator algorithms, etc.) and advanced surrogate models (deep learning models, multiple-learning machine models, etc.) in the future. In addition, the findings of the flexible mechanism reliability evaluation based on the current methods should be validated and tested by experiments to improve the applicability.

Author Contributions: Conceptualization, C.Z. and C.F.; methodology, C.Z. and H.L.; software, Z.Y. and J.W.; validation, C.Z., S.Z. and C.F.; formal analysis, C.Z. and Z.Y.; investigation, C.Z. and Z.Y.; resources, C.Z.; data curation, Z.Y. and H.L.; writing—original draft preparation, Z.Y., H.L., J.W. and S.Z.; writing—review and editing, C.F., C.Z. and J.W.; visualization, S.Z.; supervision, C.Z. and C.F.; project administration, C.Z. and C.F. All authors have read and agreed to the published version of the manuscript.

Data Availability Statement: The data used to support the findings of this study are included within the article.

Conflicts of Interest: The authors declare no conflict of interest. The funders had no role in the design of the study; in the collection, analyses, or interpretation of data; in the writing of the manuscript; or in the decision to publish the results.

References

1. Kim, S.; Na, S. Response surface method using vector projected sampling points. *Struct. Saf.* **1997**, *19*, 3–19. [CrossRef]
2. Ren, Y.; Bai, G. Determination of Optimal SVM Parameters by Using GA/PSO. *J. Comput.* **2010**, *5*, 1160–1168. [CrossRef]
3. Guo, Z.; Bai, G. Application of Least Squares Support Vector Machine for Regression to Reliability Analysis. *Chin. J. Aeronaut.* **2009**, *22*, 160–166. [CrossRef]
4. Niu, L.; Tu, H.; Dong, H.; Yan, N. Separation Reliability Analysis for the Low-Shock Separation Nut with Mechanism Motion Failure Mode. *Aerospace* **2022**, *9*, 156. [CrossRef]
5. Ren, Y.; Bai, G. New Neural Network Response Surface Methods for Reliability Analysis. *Chin. J. Aeronaut.* **2011**, *24*, 25–31. [CrossRef]
6. Isukapalli, S.S.; Roy, A.; Georgopoulos, P.G. Stochastic Response Surface Methods (SRSMs) for Uncertainty Propagation: Application to Environmental and Biological Systems. *Risk Anal.* **2006**, *18*, 351–363. [CrossRef]
7. Zhang, C.; Bai, G. Extremum response surface method of reliability analysis on two-link flexible robot manipulator. *J. Cent. South Univ.* **2012**, *19*, 101–107. [CrossRef]
8. Chen, Z.; Lu, Z.; Feng, K. A novel learning function of adaptively updating Kriging model for reliability analysis under fuzzy uncertainty. *Struct. Multidiscip. Optim.* **2023**, *66*, 135. [CrossRef]
9. Bamrungsetthapong, W.; Pongpullponsak, A. System reliability for non-repairable multi-state series–parallel system using fuzzy Bayesian inference based on prior interval probabilities. *Int. J. Gen. Syst.* **2014**, *44*, 442–456. [CrossRef]
10. Fuh, C.; Jea, R.; Su, J. Fuzzy system reliability analysis based on level $(\lambda,1)$ interval-valued fuzzy numbers. *Inf. Sci.* **2014**, *272*, 185–197. [CrossRef]
11. Zhang, X.; Gao, H.; Li, Y.F.; Huang, H.Z. A Novel Reliability Analysis Method for Turbine Discs with the Mixture of Fuzzy and Probability-Box Variables. *Int. J. Turbo Jet-Engines* **2022**, *39*, 291–302. [CrossRef]
12. Zhang, Y.; Jia, Y.; Wu, W.; Cheng, Z.; Su, X.; Lin, A. A Diagnosis Method for the Compound Fault of Gearboxes Based on Multi-Feature and BP-AdaBoost. *Symmetry* **2020**, *12*, 461. [CrossRef]
13. Xu, Y.L.; Liu, C.L.; Lu, Z.Z. Fuzzy-Random FOSM and its Application in Low Cycle Fatigue Life Reliability Analysis of an Aeronautical Engine Turbine Disk. *Key Eng. Mater.* **2006**, *324–325*, 775–778. [CrossRef]
14. Lopez, R.H.; Torii, A.J.; Miguel, L.F.F.; Cursi, J.S. Overcoming the drawbacks of the FORM using a full characterization method. *Struct. Saf.* **2015**, *54*, 57–63. [CrossRef]
15. Eshghi, A.T.; Lee, S. Adaptive improved response surface method for reliability-based design optimization. *Eng. Optim.* **2019**, *51*, 2011–2029. [CrossRef]

16. Zhu, B.; Pei, H.; Yang, Q. An intelligent response surface method for analyzing slope reliability based on Gaussian process regression. *Int. J. Numer. Anal. Methods Geomech.* **2019**, *43*, 2431–2448. [CrossRef]

17. Fei, C.W.; Choy, Y.S.; Hu, D.Y.; Bai, G.C.; Tang, W.Z. Transient probabilistic analysis for turbine blade-tip radial clearance with multi-component and multi-physics fields based on DCERSM. *Aerosp. Sci. Technol.* **2016**, *50*, 62–70. [CrossRef]

18. Zhai, X.; Fei, C.W.; Choy, Y.S.; Wang, J.J. A stochastic model updating strategy-based improved response surface model and advanced Monte Carlo simulation. *Mech. Syst. Signal Process.* **2017**, *82*, 323–338. [CrossRef]

19. Du, J.; Li, H. Direct integration method based on dual neural networks to solve the structural reliability of fuzzy failure criteria. *Proc. Inst. Mech. Eng. Part C J. Mech. Eng. Sci.* **2019**, *233*, 7183–7196. [CrossRef]

20. Yan, W.X.; Pin, W.; He, L. Reliability Prediction of CNC Machine Tool Spindle Based on Optimized Cascade Feedforward Neural Network. *IEEE Access* **2021**, *9*, 60682–60688. [CrossRef]

21. Abbasi, F.; Allahviranloo, T. Fuzzy reliability estimation using the new operations of transmission average on Rational-linear patchy fuzzy numbers. *Soft Comput.* **2019**, *23*, 3383–3396. [CrossRef]

22. Nie, X.; Li, H. Fuzzy Reliability Analysis With Fuzzy Random Variables Based on Perturbation Principle. *IEEE Access* **2019**, *7*, 78898–78908. [CrossRef]

23. Zhang, C.; Wei, J.; Jing, H.; Fei, C.; Tang, W. Reliability-Based Low Fatigue Life Analysis of Turbine Blisk with Generalized Regression Extreme Neural Network Method. *Materials* **2019**, *12*, 1545. [CrossRef] [PubMed]

24. Zhang, C.; Song, L.; Fei, C.; Lu, C.; Xie, Y. Advanced multiple response surface method of sensitivity analysis for turbine blisk reliability with multi-physics coupling. *Chin. J. Aeronaut.* **2016**, *29*, 962–971. [CrossRef]

25. Zhang, C.Y.; Wei, J.S.; Wang, Z.; Yuan, Z.S.; Fei, C.W.; Lu, C. Creep-Based Reliability Evaluation of Turbine Blade-Tip Clearance with Novel Neural Network Regression. *Materials* **2019**, *12*, 3552. [CrossRef]

26. Keshtegar, B.; Bagheri, M.; Fei, C.W.; Lu, C.; Taylan, O.; Thai, D.K. Multi-extremum modified response basis model for nonlinear response prediction of dynamic turbine blisk. *Eng. Comput.* **2022**, *38*, 1243–1254. [CrossRef]

27. Li, X.Q.; Bai, G.C.; Song, L.K.; Wen, J. Fatigue reliability estimation framework for turbine rotor using multi-agent collaborative modeling. *Structures* **2021**, *29*, 1967–1978. [CrossRef]

28. Song, L.; Bai, G.; Fei, C. Multi-failure probabilistic design for turbine bladed disks using neural network regression with distributed collaborative strategy. *Aerosp. Sci. Technol.* **2019**, *92*, 464–477. [CrossRef]

29. Song, L.; Bai, G.; Li, X. A novel metamodeling approach for probabilistic LCF estimation of turbine disk. *Eng. Fail. Anal.* **2021**, *120*, 105074. [CrossRef]

30. Yang, Y.; Xu, X.; Zhang, W. Design neural networks based fuzzy logic. *Fuzzy Sets Syst.* **2000**, *114*, 325–328. [CrossRef]

31. Li, H.; Lee, E.S. Interpolation functions of feedforward neural networks. *Comput. Math. Appl.* **2003**, *46*, 1861–1874. [CrossRef]

32. Kobayashi, M. Storage capacity of hyperbolic Hopfield neural networks. *Neurocomputing* **2019**, *369*, 185–190. [CrossRef]

33. Aengchuan, P.; Phruksaphanrat, B. Comparison of fuzzy inference system (FIS), FIS with artificial neural networks (FIS + ANN) and FIS with adaptive neuro-fuzzy inference system (FIS + ANFIS) for inventory control. *J. Intell. Manuf.* **2018**, *29*, 905–923. [CrossRef]

34. Okwu, M.O.; Adetunji, O. A comparative study of artificial neural network (ANN) and adaptive neuro-fuzzy inference system (ANFIS) models in distribution system with nondeterministic inputs. *Int. J. Eng. Bus. Manag.* **2018**, *10*, 1655968150. [CrossRef]

35. Jang, J.S.R. ANFIS: Adaptive-network-based fuzzy inference system. *IEEE Trans. Syst. Man Cybern.* **1993**, *23*, 665–685. [CrossRef]

36. Ren, Y.; Liu, F.; Lv, J.; Meng, A.; Wen, Y. T-S fuzzy systems optimization identification based on FCM and PSO. *EURASIP J. Adv. Signal Process.* **2020**, *2020*, 47. [CrossRef]

37. Yao, S.B.; Luo, Z.; Wei, K.; Sun, Y.H.; Xu, C.Y. Analysis of fluid-solid-thermal coupling characteristics of axial-symmetric vectoring exhaust nozzle. *Proc. Inst. Mech. Eng. Part C J. Mech. Eng. Sci.* **2022**, *236*, 9472–9484. [CrossRef]